Journal of Power Sources 273 (2015) 255–263

Contents lists available at ScienceDirect

Journal of Power Sources

journal homepage: www.elsevier.com/locate/jpowsour

Current sensor-less state-of-charge estimation algorithm for lithium-ion batteries utilizing filtered terminal voltage

Chang Yoon Chun [a], Jongbok Baek [a], Gab-Su Seo [a], B.H. Cho [a, *], Jonghoon Kim [b], Il Kwon Chang [c], Sangwoo Lee [c]

[a] Department of Electrical and Computer Engineering, Seoul National University, Seoul 151-744, Republic of Korea
[b] Department of Electrical Engineering, Chosun University, Gwangju, Republic of Korea
[c] Silicon Mitus, Inc., Gyeonggi-do, Republic of Korea

HIGHLIGHTS

- This paper proposes state-of-charge estimation algorithms without sensing the current.
- The estimation performance due to the model's accuracy is investigated.
- The aspect of the SOC estimation error in accordance with battery usage is analyzed.
- Discussions on battery modeling and detailed parameter extraction steps are provided.
- The proposed algorithms are simple to implement and easy to use for portable devices.

ARTICLE INFO

Article history:
Received 4 July 2014
Received in revised form
27 August 2014
Accepted 28 August 2014
Available online 16 September 2014

Keywords:
Battery fuel gauge
Filtered terminal voltage
Lithium-ion batteries
Monte Carlo simulation
State estimation
State-of-charge (SOC)

ABSTRACT

This paper proposes state-of-charge (SOC) estimation algorithms that utilize a filtered battery terminal voltage without measuring the current. These methods extract an estimated open-circuit voltage (OCV) or current from the battery terminal voltage through equivalent circuit model-based filters, which streamlines the estimation process. In the methods, the OCV values derived from the corresponding SOCs are used to extract the filter coefficient for ease of implementation. The relationship between the model's accuracy and estimation performance is investigated, and the variation of the SOC estimation error due to the model parameter tolerance is also derived by the Monte Carlo simulation tool to confirm the practicality of the method. To validate the performance of the proposed approach, a parameter extraction profile and an actual mobile phone profile are applied to a 2.6 Ah prismatic Li-ion battery. The experimental results show the feasibility of the proposed SOC estimation algorithm to within a 5% SOC estimation error.

1. Introduction

Lithium-based batteries feature a higher voltage, higher energy density, lower self-discharge, and longer cycle life than other secondary batteries. These characteristics make the Li-based batteries useful for many applications such as portable devices, electric vehicles (EVs), and energy storage systems (ESS) [1,2]. In such applications, an accurate estimation of a state-of-charge (SOC) is critical to use the battery continuously without damage. A precise SOC indicates the battery runtime and charge/discharge condition; it also prevents unexpected shutdowns by estimation errors [3,4]. Especially in portable devices where a single battery or a small size battery pack is used as a power source, such as mobile phones, digital cameras, and laptop computers, extending the battery runtime and minimizing the circuit area are also crucial factors.

A great deal of research has gone into achieving “accurate” SOC estimation. Coulomb counting method is widely used, because of its intuitive relationship of the SOC and battery capacity and also because of high performance in short-term SOC changes [4–6]. However, it intrinsically has an initial SOC error and accumulated sensing error problems caused by time integration of the current. On the opposite, numerical methods such as the OCV method, neural network, and fuzzy logic are free of the initial and cumulative error issues, but the estimated SOC may fluctuate, due to

* Corresponding author. Tel.: +82 2 880 1785; fax: +82 2 878 1452.
E-mail address: bhcho@snu.ac.kr (B.H. Cho).

http://dx.doi.org/10.1016/j.jpowsour.2014.08.121
0378-7753/

disturbances to the model's sensitivity [7–9]. To optimally achieve the both advantages of the Coulomb counting and numerical methods, adaptive methods such as an extended Kalman filter (EKF), unscented Kalman filter (UKF), and other nonlinear particle filters have been studied in recent years [10–13]. These adaptive SOC estimation methods give more accurate results, while they carry a considerable computational burden. However, these approaches use the battery current information, which would not be suitable in portable devices systems due to the power dissipation in the current sensing network and size and cost constraints.

This paper proposes SOC estimation methods without current measurement utilizing the estimated OCV and estimated current information from the filtered terminal voltage. The OCV values, in accordance with the particular SOC values, are naturally obtained from the proposed parameter extraction process and directly used to set the filter coefficients. To analyze their performance with respect to parameter tolerance of the simple RC battery model, a Monte Carlo simulation is carried out for SOC error. Also, the experimental SOC estimation verifies validity of the proposed method by showing the estimation error within 5% and thus suitability for portable devices.

The rest of this paper is organized as follows: Section 2 presents the battery modeling and its parameter extraction. Section 3 describes the battery SOC estimation algorithm for Li-ion batteries without using the battery current information. The influence of the parameter tolerance in the SOC estimation algorithm and the variation in error during rest periods are discussed in Section 4. In Section 5, experimental test procedures and results are provided for verification of the proposed approach. The final section summarizes the paper.

2. Battery modeling and parameter extraction

2.1. Battery modeling

Battery modeling plays an important role in the battery's SOC estimation, regardless of the estimation methods. Coulomb counting uses the battery model as a compensation index to suppress the accumulative current error. Other methods use the battery model to estimate the battery's SOC through the relationship between the terminal voltage, current, and battery SOC information. Thus, the accuracy of the battery model affects the performance of the battery SOC estimation.

To establish battery models, several papers have focused on the electrochemical characteristics [14–16] or terminal voltage response of battery [13,17–20]. The electrochemical models are expressed by mathematical equations that represent the battery's chemical properties and the model coefficient should be derived from empirical data, in order to complete the model. On the other hand, the equivalent circuit models use electric circuit parameters such as resistances, capacitances, and voltage sources to express the battery terminal voltage response to applied current. Although the detailed and complicated models can improve the accuracy of modeling, they increase the computational burden and memory requirements of the system in formulating the battery's nonlinear characteristics. In this paper, the equivalent circuit models are used for a relatively simple parameterization process and a small number of mathematical formulas compared to the electrochemical models.

There are many equivalent circuit models that have accomplished a goal to express the terminal voltage characteristics by using a variety of circuit structures [18–21]. However, due to the nature of Thevenin's theorem, these equivalent circuit models typically have similar forms comprising a voltage source and internal impedance. First, this voltage source is modeled as a simple capacitor or a dependent voltage source that follows an OCV–SOC relationship. If the OCV–SOC relationship of the battery is linear, then the battery can be simply modeled as a capacitor; however, if the OCV–SOC relationship is piecewise linear, as shown in Fig. 1, the capacitance needs to be varied in a particular SOC region. Second, the internal impedance in the models is expressed in different ways to represent dynamic effects such as terminal voltage relaxation. Focusing on the number of the resistor-capacitor (RC) ladders, three impedance models are described in this paper as follows: a simple battery model that has a resistor (Fig. 2(a)), a Thevenin battery model that has a resistor and a single RC (1-RC) ladder (Fig. 2(b)), and an impedance model that has a resistor and three RC (3-RC) ladders (Fig. 2(c)) [22,23]. For minimizing the memory increment in detailed models, the relation between RC parameter and the number of RC ladders is applied from the Warburg impedance in a Randles model, which is described in Fig. 3 [24,25]. Thus, all impedance models can be specified by up to three internal parameters, which are the series resistance, R_i, and the resistance and capacitance of the RC ladder, R_{diff} and C_{diff}, as shown in Fig. 2. In order to analyze the model suitability in estimating the SOC of the portable devices, these models are used to examine the link between the complexity of the models and the performance of the algorithms in Section 3.

2.2. Parameter extraction

The proposed model contains the maximum three internal impedance parameters and the OCV–SOC relationship. Each parameter extraction step is described as follows:

(1) Experimental Setup: The target battery was a Samsung SDI prismatic Li-ion battery with a rated voltage of 3.85 V and a rated capacity of 2600 mAh (for Samsung Galaxy S4). The experimental setup consisted of a power supply (Agilent E3633A), an electronic load (Hewlett Packard 6050A), and the current sensing network (precision resistors). A personal computer controlled the power supply and electronic load, and it collected the battery terminal voltage and current information through an NI data acquisition board.
(2) Capacity determination: Typically, a battery capacity depends on the magnitude of discharge current. For this reason, the rated capacity in a battery datasheet is defined by fully-charging and fully-discharging batteries in a specific C-rate, which is the normalized charge or discharge current against the battery capacity. In case of the target cell, the same procedure measuring the rated capacity in the datasheet was used. The charging and discharging cut-off voltage were set to 4.35 V and 2.75 V, respectively. In the battery charging

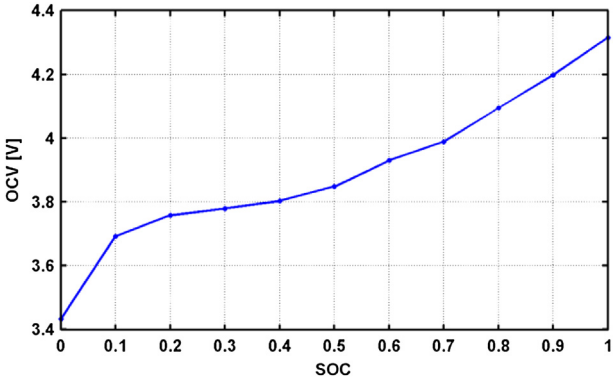

Fig. 1. Battery OCV–SOC curve.

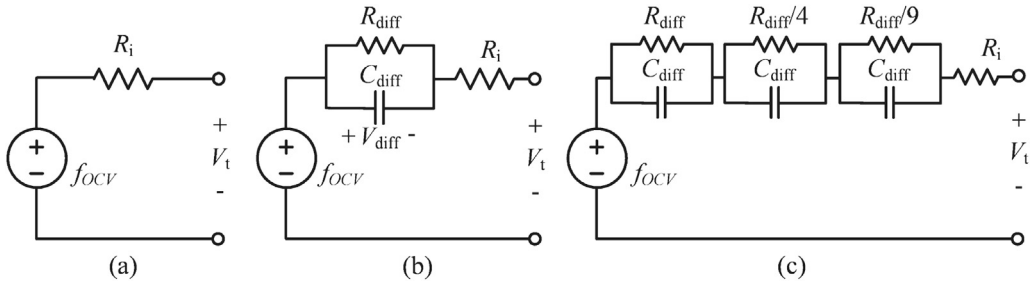

Fig. 2. The proposed equivalent circuit models: (a) Simple model, (b) Thevenin model, and (c) Impedance model.

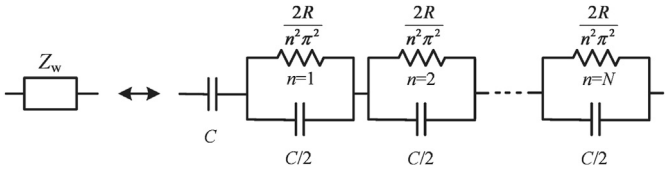

Fig. 3. Warburg impedance.

period, a constant current–constant voltage (CC–CV) mode was used. The charging process starts with 0.2 C (520 mA) during CC mode, and ends with 0.05 C (130 mA) at CV mode after the battery voltage reached to the charging cut-off. After the charging process, the discharging process is conducted with the same 0.2 C (520 mA) during CC mode to the discharging cut-off. According to the duration time and the current information, the capacity of the target battery was experimentally obtained as demonstrated in Fig. 4. In this capacity determination process, the sensing gain of current information amplifies the white Gaussian noise in analog-to-digital conversion (ADC) as shown in Fig. 4(a). For experimental reproducibility, the end of charging/discharging experimental condition should be same through the moving average of battery voltage and current information. Otherwise, current oscillation that influences the end of experimental charging condition results in erroneous capacity determination and unexpected parameters extraction.

(3) OCV–SOC curves: From the calculated battery capacity, the OCV values were experimentally extracted at every 10% SOC interval by discharging 10% of the battery capacity with the same 0.2 C (520 mA). After each 10% discharging, 1-h rest, during which charging or discharging does not occur, was applied to obtain the OCV as shown in Fig. 4. From these OCV values corresponding to 10% SOC interval, an additional process of linear interpolation was conducted to obtain a slope and a *y*-intercept of each interval OCV-SOC curve.

(4) Battery parameters: The impedances were measured by the 1-h rest period of the OCV–SOC extraction step with the direct current internal resistance (DCIR) [13,26]. The parameters were obtained by comparing the battery impedance described in (1) and the voltage response during the rest interval shown in Fig. 5. The parameters might be varied according to the SOC range, but in this paper, the averaged value of the parameters obtained from the middle SOC range were used, because the parameters have similar values in most of the SOC region. Table 1 shows the parameters obtained through the aforementioned methods and identified that the total resistances of each model were equal to all three types of the equivalent circuit model.

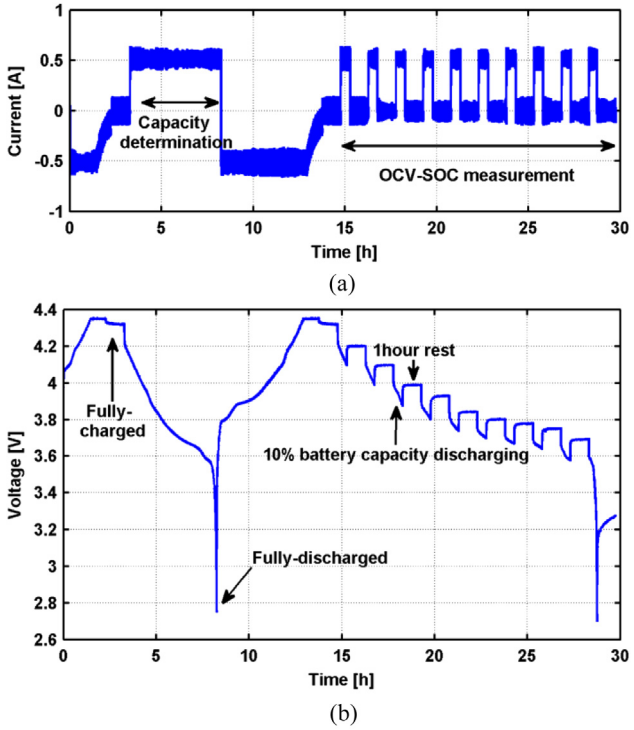

Fig. 4. Capacity determination and OCV–SOC measurement steps: (a) Current profile, (b) Voltage response.

3. SOC estimation (fuel gauge) algorithms utilizing filtered terminal voltage

3.1. Proposed SOC estimation algorithms

The battery parameter can be measured through electrochemical impedance spectroscopy (EIS), which applies an AC potential to an electrochemical cell and then measures the current through the cell (potentiostatic mode) [24]. From the ratio between

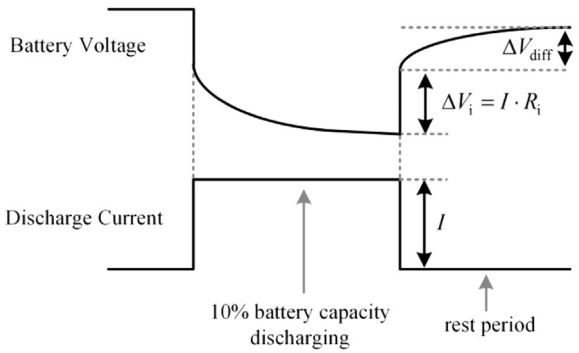

Fig. 5. The parameter extraction at rest period using DCIR and the battery time constant.

Table 1
Extracted parameters of the three proposed equivalent circuit models.

Model types	Series resistance R_i [Ω]	Diffusion resistance R_{diff} [Ω]	Diffusion capacitance C_{diff} [F]	Total resistance [Ω]
Simple model	0.201			0.201
Thevenin model	0.147	0.0538	6980	0.201
Impedance model	0.128	0.0538	6980	0.201

the applied voltage and resultant current information in a certain frequency range, the battery impedance can be obtained and represented as a model parameter such as the series resistance, RC ladder, and OCV after passing through a specific frequency filter [27–30]. In other words, there is a relationship between the voltage and current of a specific frequency, and the battery model parameter. Based on this relationship, a research study has been performed to estimate the OCV without the current information [17]. The proposed method use the linear interpolation of OCV values corresponding to particular SOCs from model parameter extraction. Thus, the filter coefficients can be derived easier than that in Ref. [17] because it require additional calibration process to obtain constant filter coefficients corresponding to a particular OCV region. Besides using this intuitive technique, not only the estimated OCV but also the estimated current can be derived through this relationship, which enables SOC estimation in two different ways.

In this paper, the operating principles and the performance of the overall SOC estimation algorithms that use the specific frequency filtered terminal voltage are described. From the battery model described in Section 2, the simplest battery model consists of a single resistor and a single capacitor represented by the OCV–SOC relationship. When the battery model consists of passive elements such as a resistor R and a capacitor C in Fig. 6, the capacitor voltage V_c and the resistor voltage V_R can be calculated by the terminal voltage V_t divided by the impedance ratio. In other words, the equivalent capacitor voltage and the equivalent resistor voltage (V_c and V_R in Fig. 6) can be obtained when the terminal voltage is passed through a low-pass filter (LPF) and a high-pass filter (HPF), respectively. The relationships mentioned above can be represented in Laplace notation in Eqs. (1) and (2).

$$\frac{V_c}{V_t} = \frac{1}{1+sRC} \tag{1}$$

$$\frac{V_R}{V_t} = \frac{sRC}{1+sRC} \tag{2}$$

In order to implement this algorithm in a digital processor and minimize the amount of memory, the processes of transforming Eq. (1) into the time domain and discretizing the differential equation using Eq. (3), where T_s is the sampling time, are needed. Thus, a discrete-time and a recursive representation form of Eq. (1) is shown as Eq. (4) and the coefficient α in Eq. (4) is defined as the smoothing factor in Eq. (5).

$$\frac{dV_c}{dt} \approx \frac{V_c[k] - V_c[k-1]}{T_s} \tag{3}$$

$$V_c[k] = V_c[k-1]\cdot(1-\alpha) + V_t[k]\cdot\alpha \tag{4}$$

$$\alpha = \frac{T_s}{T_s + RC} \tag{5}$$

Based on the relationship between the estimated resistor voltage and current, Eq. (2) can be transformed to Eq. (6). If the same procedure in estimated capacitor voltage is applied to Eq. (6), the estimated current information, I, can be obtained in Eq. (7).

$$\frac{I}{V_t} = -\frac{sC}{1+sRC} \tag{6}$$

$$I[k] = (1-\alpha)\cdot\left(I[k-1] + \frac{(V_t[k] - V_t[k-1])}{R}\right) \tag{7}$$

As described in Eq. (4), the estimated capacitor voltage refers to the battery OCV. This means that these proposed algorithms using LPF or HPF obtain the estimated OCV and the estimated current value, respectively.

From Eq. (8) (Ohm's law for a capacitor) and the differential equation form of SOC definition in Eq. (9), the relationship between the capacitance, C, the battery capacity, C_n, and the OCV–SOC relationship is derived in Eq. (10), because the capacitor voltage is considered as OCV. Thus, the capacitor in the RC battery model, as shown in Fig. 6, can be regarded as a variable capacitor according to the slope of the OCV–SOC curve.

$$I = -C\frac{dV_c}{dt} \tag{8}$$

$$\frac{dSOC}{dt} = -\frac{I}{C_n} \tag{9}$$

$$C = C_n\frac{dSOC}{dOCV} \tag{10}$$

In order to use the estimated current information, an initial SOC is necessary. The initial SOC is obtained from the OCV–SOC relationship, by letting initial terminal voltage as the initial OCV. From this SOC information and Eq. (9), the battery SOC is calculated by using the Coulomb counting method.

Summarizing the above steps, Fig. 7 is the flow chart of the proposed SOC estimation algorithms that use the current and OCV information based on the filtered terminal voltage. Directly obtaining the OCV from the estimated SOC is a relatively simple process compared to obtaining the SOC from a specific OCV, it is thus noted that the proposed method let the capacitance C be easily derived, which makes the estimation process simpler and cost-effective.

3.2. Performance of the estimation algorithms

In order to estimate a more accurate SOC, more sophisticated models are inevitably required. In Section 2, three different battery impedance models are described such as a simple resistor, a Thevenin with a resistor and 1-RC ladder, and an impedance model with a resistor and 3-RC ladders. In terms of SOC estimation accuracy, their performances are analyzed by observing the dynamic responses.

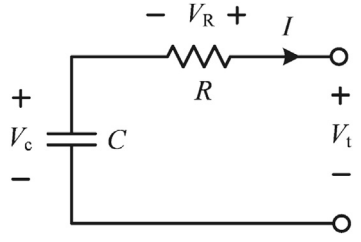

Fig. 6. Simple RC battery model.

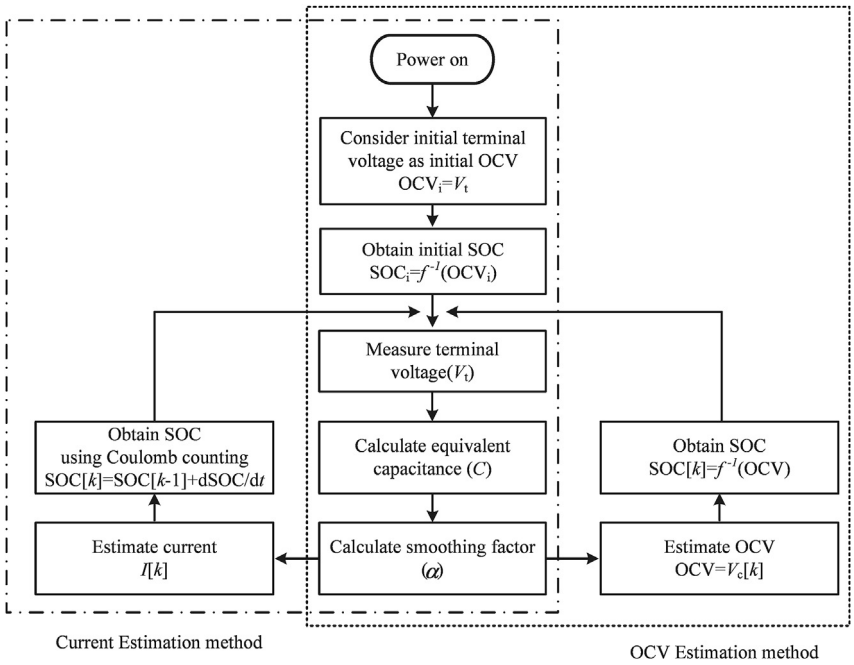

Fig. 7. The flow chart of the SOC estimation algorithm using filtered terminal voltage: (a) Current estimation, (b) OCV estimation.

Performing the same procedure for performance comparison, the three LPF relationships between these battery impedance models and the variable capacitor are analyzed. To analyze their dynamics, the Bode plots of these LPF models are presented in Fig. 8. In this analysis, model parameters listed in Table 1 and the averaged slope of the OCV–SOC curve in the SOC region from 70 to 100% are adopted as a representative values. While the magnitude of the Bode plot is almost the same in the range from low frequency to around cut-off frequency region, in a high frequency range, the gain difference increases due to the differences in the RC ladder model. These model errors affect the performance of the SOC estimation because the algorithm could not quickly respond to short-term SOC variation. On the contrary, long-term SOC trends of the models would be similar due to the identical low frequency characteristics.

As mentioned in Eqs. (4), (5), (8) and (10), the battery SOC variation per each sampling, K_{est}, is derived as

$$K_{est} = \frac{dSOC}{dt} = \frac{dSOC}{dOCV}\cdot\frac{dOCV}{dt} \approx \frac{1}{RC_n}\cdot(V_t[k] - V_c[k-1]). \quad (11)$$

Assuming that the battery is discharged with a constant current, then K_{est} should have a constant value. To satisfy this condition, the resistance, R, should change depending on the distance between the terminal voltage and the OCV. However, if the R is fixed in the simple RC model in Fig. 2(a), the R value is relatively high in the high frequency range, and it makes the K_{est} and estimated current smaller at instantaneous voltage changes, as shown in Fig. 9. Therefore, if the system requires a simple algorithm and can endure the short-term SOC error, a simple battery model is sufficient. Otherwise, a complicated battery model is needed in order to satisfy the system conditions.

The OCV and current estimation algorithms use the same formula except Eqs. (1) and (2). These two equations inform the same information, because the sum of the estimated capacitor voltage V_c and the estimated resistor voltage V_R is equal to the terminal voltage V_t. For this reason, the SOC estimation results obtained by the OCV and current estimation can be predicted as the same, and it is easy to identify both performances when a single estimation method is checked. As an example, the current is estimated using the inaccurate model and the battery capacity, which is varied under the current magnitude in Eq. (10). An SOC estimation error can occur due to this current estimation error, but after sufficient rest time, the SOC estimation error will be automatically reduced as in the OCV estimation method. In other words, the estimated current is not an actual value; the estimated current is corrected using OCV information.

4. Parameter tolerance and error estimation

The proposed SOC estimation algorithms described in Section 3 have advantages such as the convenience of implementation and

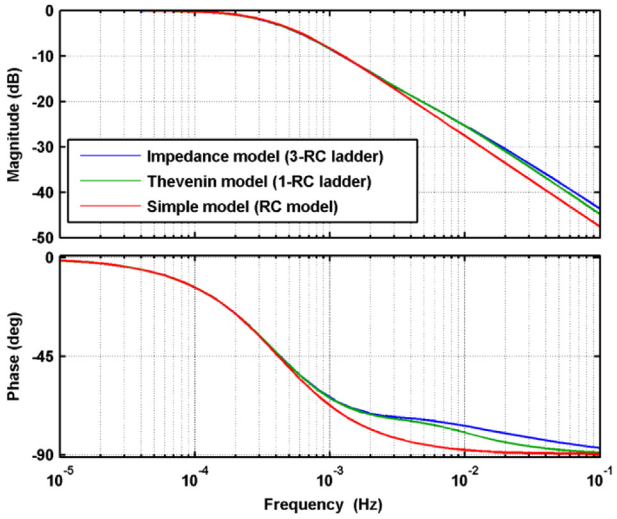

Fig. 8. The Bode plot of each model according to the LPF in the SOC region from 70 to 100%.

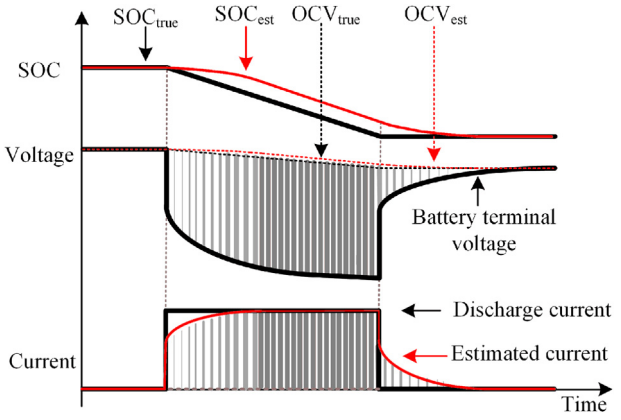

Fig. 9. SOC and current estimation performance due to the limitations in a simple RC model.

the simplicity of the algorithms. On the other hand, because there is no current sensing information, it is limited to directly update the battery parameters when a gap occurs between the values of the parameters in the algorithm and the actual ones, which would cause estimation errors. Especially in mass produced products such as portable devices, variations between the battery parameters inevitably exist even though the battery screening process [31] precedes to minimize them, and it is not practical to directly adjust the parameters to match the characteristics of each device. To observe the effects of parameter tolerance and confirm the practicality of the proposed methods, this section provides a practical analysis using a randomized algorithm.

In SOC estimation, sensing noise (in obtaining battery information) and parameter tolerances can affect the performance of a method. The sensing noise of the battery voltage has less influence on the SOC fluctuation or chattering compared to the normal battery model-based algorithm because the proposed estimation algorithms directly filter the battery's terminal voltage information. On the other hand, the SOC estimation error might be affected by the parameter tolerances, which indicate the possibility of the differences between the actual measured parameters (RC parameters, OCV, battery capacity) of the battery and the parameters used in the algorithm. For observing the phenomenon on the SOC estimation error resulting from the parameter variations, a Monte Carlo simulation with 100 trials is carried out to provide statistical worst-case analysis.

To carry out a valid simulation, a mathematical equation is derived from the previous analysis. From Eq. (11), the SOC estimation error, E, when the battery is constantly charging/discharging in a certain SOC variation, K_{true}, can be estimated as.

$$E = \mathrm{SOC}_{true} - \mathrm{SOC}_{est} = E_i + \int (K_{true} - K_{est})\mathrm{d}t \tag{12}$$

where SOC_{true} and SOC_{est} are the true and estimated SOC, and E_i is the initial SOC estimation error. For calculating the SOC estimation error from the Eqs. (11) and (12), the process of obtaining the terminal voltage, V_t, from K_{true} is additionally needed since the E_i and K_{true} are decided in simulation. To find the terminal voltage with simple calculation, the battery model shown in Fig. 2(b), which is a more complex form, is used. This allows the terminal and RC ladder voltages (V_t, V_{diff}) can be represented as Eqs. (13) and (14), where f_{OCV}, R_i, R_{diff}, and C_{diff} are a function of OCV according to the SOC, series resistor, diffusion resistor, and diffusion capacitor, respectively.

$$V_t[k] = f_{OCV}(\mathrm{SOC}_{true}) - R_i \cdot (-K_{true} C_n) - V_{diff}[k] \tag{13}$$

$$V_{diff}[k] = \left(1 - \frac{T_s}{R_{diff} C_{diff}}\right) \cdot V_{diff}[k-1] + \frac{1}{C_{diff}} \cdot (-K_{true} C_n) \tag{14}$$

It is assumed that the initial value of the actual and estimated SOC are random variables with uniform distribution, and that the internal resistance and battery capacity in the estimation algorithm are random variables with Gaussian distribution as shown in Fig. 10. The average values of the internal resistance and battery capacity are regarded as the actual battery parameters, and the tolerances are set to 30% and 5% respectively. If there is no difference between the actual measured OCV–SOC and the OCV–SOC used in the algorithm, an SOC estimation error due to parameter tolerance will automatically decrease after sufficient rest time. In the presence of an initial SOC estimation error, Fig. 11 shows the flow of the SOC estimation error and time until the error is within 5% during the rest period. As a result, it is confirmed that the SOC will stays within the 5% error bound if the battery is not used for about 100 min.

The SOC estimation error occurs when a difference exists between K_{est} and K_{true} due to the RC parameter tolerance. This means that the OCV estimation or current estimation method using the terminal voltage could be incorrect. However, the error may not continue to increase because the slope difference between K_{est} and K_{true} is limited to a specific bound and reduced as shown in Fig. 9. In other words, the K_{est} can be changed to obtain a constant distance across the terminal voltage and the estimated OCV from Eq. (11). Based on this information, the maximum magnitude of the SOC estimation error using the same parameter as mentioned above is simulated and calculated. Fig. 12 shows that the maximum error values are proportional to the amount of the current. Thus, the error converged to a certain value when the battery was charged or discharged with a constant current.

The RC parameter tolerance affects the instantaneous SOC error, which will disappear over sufficient time, but the OCV–SOC curve parameter permanently affects the error. Fig. 13(a) shows the distribution of OCV–SOC curves in the estimation algorithm when the same Monte Carlo simulation was conducted. If a difference between the OCV–SOC curve in the algorithm and a real battery's

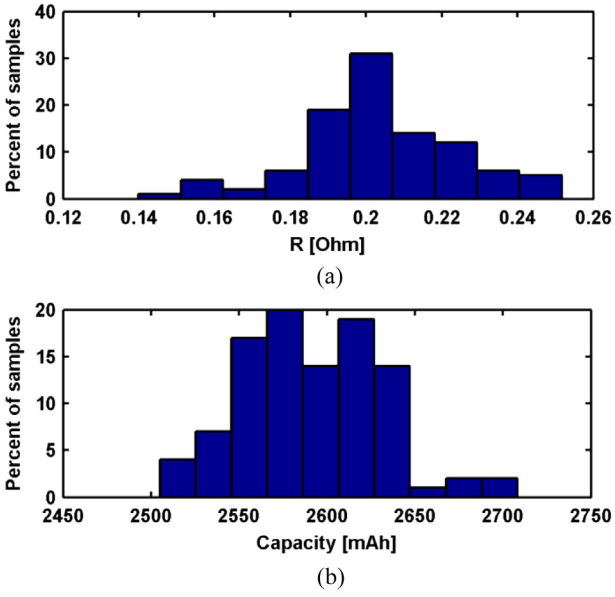

Fig. 10. Distribution of the parameters in the estimation algorithm: (a) Internal resistance, (b) Battery capacity.

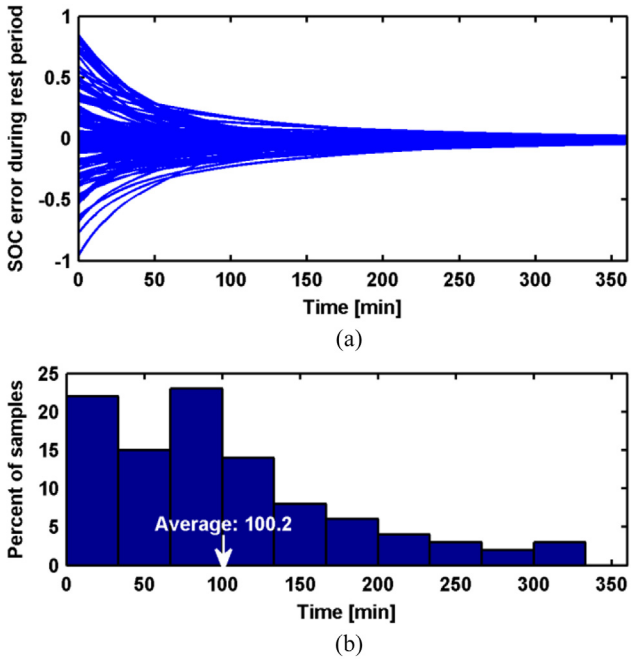

Fig. 11. Simulation of the SOC error variation during the rest period: (a) SOC error, (b) Time until the SOC error is within 5%.

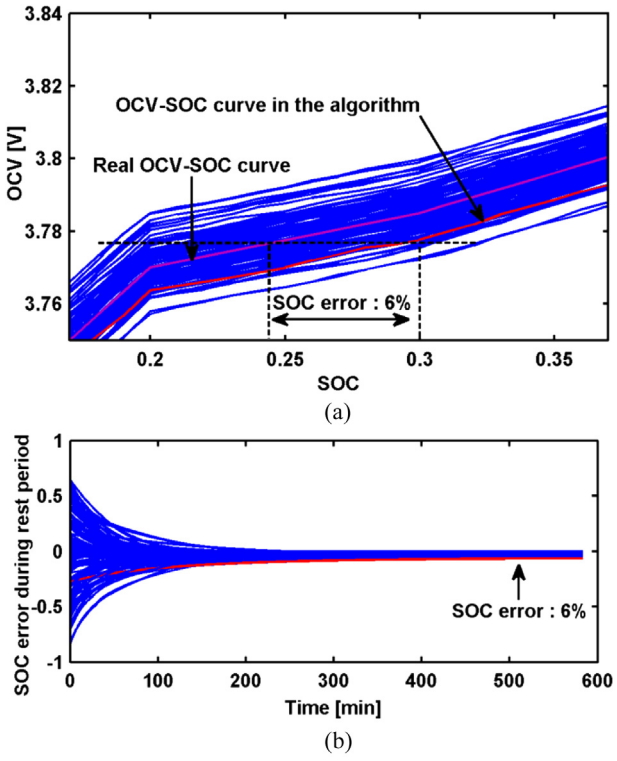

Fig. 13. (a) Distribution of OCV–SOC curve in the estimation algorithm, (b) SOC error during rest period.

OCV–SOC characteristic exists, this difference causes the permanent SOC error in the end. Assuming a 30% initial SOC error, the SOC error cannot be reduced to less than 6% even after the sufficient rest time as shown in Fig. 13(a) and (b). Thus, it is important to obtain the correct OCV–SOC relationship, especially in low-slope regions to reduce the error bounds.

In summary, although the current sensor-less SOC estimation algorithm has the drawback of its impossibility in updating the parameters directly, the error automatically decreases during rest or standby modes. For most portable devices or UPS systems, because the standby time is long enough to compensate the short-term SOC error as discussed in Section 2, these simple algorithms presented in this paper are advantageous.

5. Results and discussion

To verify the operation of the proposed SOC estimation algorithm, the same cell that was previously used for parameter extraction is used. The battery is charged under a constant current–constant voltage (CC–CV) protocol with 0.2 C (520 mA), discharged under the 0.2 C (520 mA), and rested during 1 h, as shown in Figs. 14 and 15. In this experiment, the SOC error is within a 5% bound and shows a decreasing tendency during rest periods. At the start of the experiment in particular, the initial SOC error is added, but the SOC estimation error decreases due to the relationship between the terminal voltage and the estimated OCV in Fig. 15. In the proposed current estimation method (the other way of estimating the SOC), the performance of the current estimation is low at the moment the current is abruptly changed, as shown in Fig. 16.

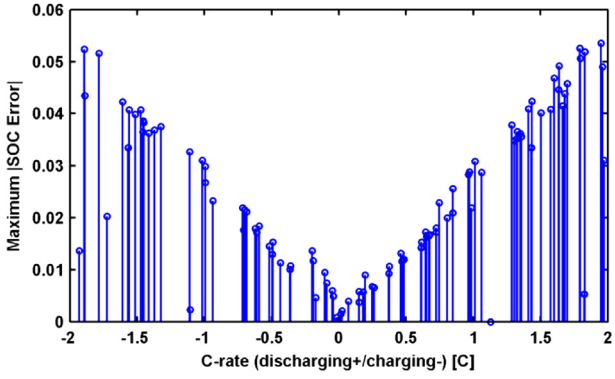

Fig. 12. Maximum magnitude of SOC estimation error under discharging/charging conditions.

To confirm that these algorithms operate properly in actual portable devices, the battery voltage and current information are measured from an actual mobile phone in Fig. 17. Before applying this current and voltage information to the SOC estimation algorithms, the resistance between the measuring port and actual battery terminal is considered. After this process, the SOC estimation result is obtained as in Fig. 18, and it shows the comparable estimation performance with the preliminary experiments in Fig. 14.

In accordance with these results, the proposed algorithms are normally operated even with the simplest battery model, and the processes of the algorithms are simple to implement. However, the parameter extraction processes are relatively complex and time-consuming, because of its long rest periods in the OCV–SOC relationship acquisition process. To alternatively solve this problem, the OCV–SOC curve can be simply obtained through averaging the battery voltages of constant current discharging and charging as shown in Fig. 19. Using this method, the resistance of the simple battery model can also be acquired from the ratio of the current and the distance between the two battery voltages. However, this method has limitations, as the OCV–SOC model error occurs at both low and high SOC ranges; thus, OCV–SOC relationship in low and

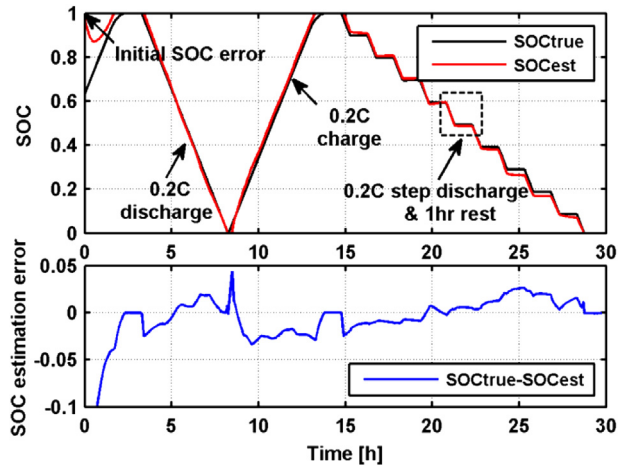

Fig. 14. SOC estimation results of applying the parameter extraction profile (Fig. 4).

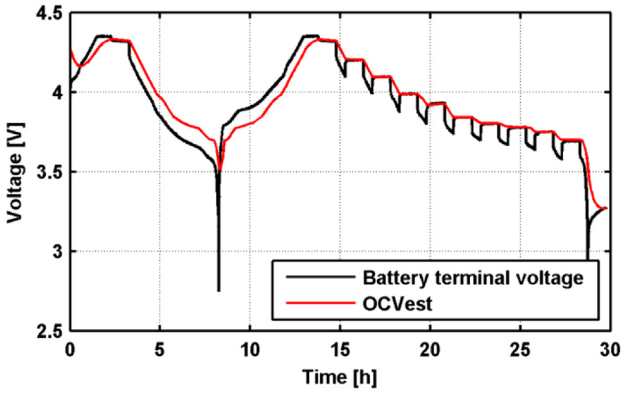

Fig. 15. Battery terminal voltage and estimated OCV of applying the parameter extraction profile (Fig. 4).

high SOC range needs to be supplemented. Despite this drawback, it can easily identify the approximate tendencies of OCV–SOC curve compared to the OCV–SOC extraction with 10% rest period in most of the SOC region. These trends show the inflection points of changing the OCV–SOC curve slope which divide the specific SOC intervals rather than 10% equal intervals. Consequently, the two parameter extraction methods are used in a mutually complementary manner and in conformity to the objectives such as accuracy and convenience.

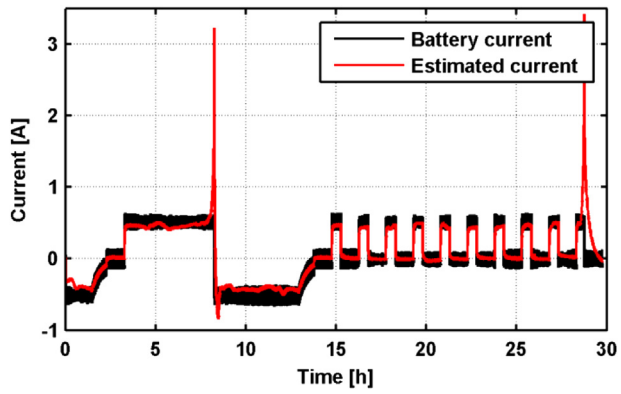

Fig. 16. Battery measured and estimated current of applying the parameter extraction profile (Fig. 4).

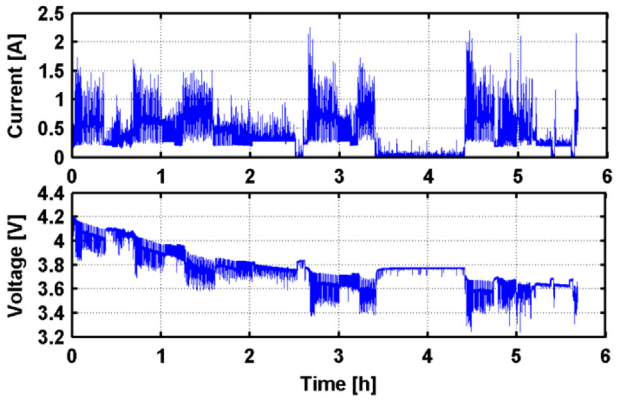

Fig. 17. Measured battery voltage and current from actual mobile phone load profile.

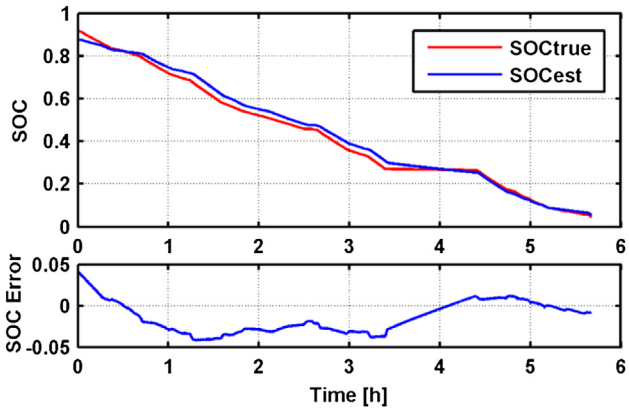

Fig. 18. SOC estimation result of applying the actual mobile phone load profile (Fig. 17).

6. Conclusion

In portable devices using a single or small-sized battery, simplicity and low power dissipation of the SOC estimation process are as important factors as the precise SOC estimation. To achieve these goals, the OCV and current estimation methods for obtaining the SOC are presented, utilizing the filtered battery terminal voltage without measuring the current. Without current sensor, it is not necessary to consider the current offset or current sensing gain errors, and the power dissipation in the current sensor and the processor conducting SOC estimation should be reduced. For the

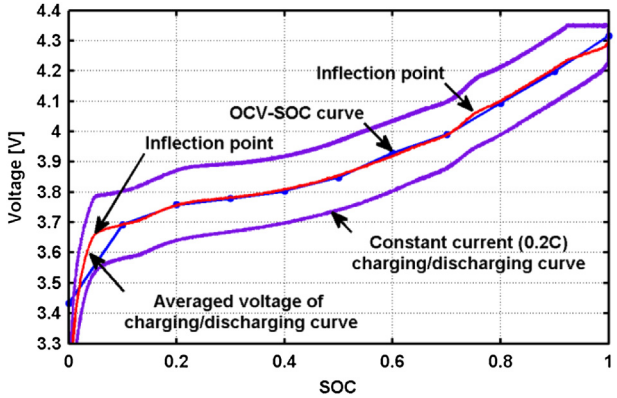

Fig. 19. Comparison between the OCV–SOC curve and the voltage of continuous charging/discharging.

easy implementation of these SOC estimation methods unlike in the previous study, the OCV values that are in accordance with the particular SOCs are used. Consequently, the algorithm can be easily implemented in hardware with fewer calibration steps, longer battery runtime, and smaller circuit area.

In addition, the relationship between the battery model and the algorithms were described to identify the characteristics and performance of the algorithms due to the model's accuracy. From these descriptions, the proposed SOC estimation error function and the SOC estimation error variation due to the RC parameter and OCV tolerance were derived using a Monte Carlo simulation. Since there is no current information, it is impossible to directly update the algorithm parameters in the proposed methods in real time, but the weakness would reduce depending on the particular use. The SOC estimation error automatically decreases during rest periods or standby mode durations regardless of the initial SOC error. Thus, the proposed algorithms have advantages such as simplicity and ease of use for use in portable devices or UPS systems.

References

[1] M.M. Thackeray, C. Wolverton, E.D. Isaacs, Energy Environ. Sci. 5 (2012) 7854–7863.
[2] T.-H. Kim, J.-S. Park, S.K. Chang, S. Choi, J.H. Ryu, H.-K. Song, Adv. Energy Mater. 2 (2012) 860–872.
[3] L. Lu, X. Han, J. Li, J. Hua, M. Ouyang, J. Power Sources 226 (2013) 272–288.
[4] K.W.E. Cheng, B.P. Divakar, H. Wu, K. Ding, H.F. Ho, IEEE Trans. Veh. Technol. 60 (2011) 76–88.
[5] M. Coleman, C.K. Lee, C. Zhu, W.G. Hurley, IEEE Trans. Ind. Electron 54 (2007) 2550–2557.
[6] K.S. Ng, C.-S. Moo, Y.-P. Chen, Y.-C. Hsieh, Appl. Energy 86 (2009) 1506–1511.
[7] H. He, X. Zhang, R. Xiong, Y. Xu, H. Guo, Energy 39 (2012) 310–318.
[8] W.X. Shen, Energy Convers. Manage 48 (2007) 433–442.
[9] P. Singh, C. Fennie Jr., D. Reisner, J. Power Sources 136 (2004) 322–333.
[10] G.L. Plett, J. Power Sources 134 (2004) 262–276.
[11] N. Watrin, R. Roche, H. Ostermann, B. Blunier, A. Miraoui, IEEE Trans. Veh. Technol. 61 (2012) 3420–3429.
[12] M. Mastali, J. Vazquez-Arenas, R. Fraser, M. Fowler, S. Afshar, M. Stevens, J. Power Sources 239 (2013) 294–307.
[13] I.-S. Kim, IEEE Trans. Power Electron 25 (2010) 1013–1022.
[14] P. Rong, M. Pedram, IEEE Trans. Very Large Scale Integr. (VLSI) Syst. 14 (2006) 441–451.
[15] V.R. Subramanian, V. Boovaragavan, V. Ramadesigan, M. Arabandi, J. Electrochem. Soc. 156 (2009) A260–A271.
[16] P.M. Gomadam, J.W. Weidner, R.A. Dougal, R.E. White, J. Power Sources 110 (2002) 267–284.
[17] J.A. Wortham, Model-based battery fuel gauges and methods, US Patent 8,198,863 B1, Jun. 12, 2012.
[18] W. Su, M.-Y. Chow, in: Proceedings of 37th Annual Conference of the IEEE Industrial Electronics Society (IECON), 2011, pp. 3248–3253.
[19] S.M. Mousavi G., M. Nikdel, Renew. Sust. Energ. Rev. 32 (2014) 477–485.
[20] M. Chen, G.A. Rincon-Mora, IEEE Trans. Energy Convers. 21 (2006) 504–511.
[21] X. Li, J. Liu, M.N. Banis, A. Lushington, R. Li, M. Cai, X. Sun, Energy Environ. Sci. 7 (2014) 768–778.
[22] M. Einhorn, F.V. Conte, C. Kral, J. Fleig, IEEE Trans. Power Electron 28 (2013) 1429–1437.
[23] J. Lee, O. Nam, B.H. Cho, J. Power Sources 174 (2007) 9–15.
[24] S. Buller, Impedance-based Simulation Models for Energy Storage Devices in Advanced Automotive Power Systems, PhD Dissertation, RWTH Aachen University, December 2002.
[25] C. Fleischer, W. Waag, H.-M. Heyn, D.U. Sauer, J. Power Sources 260 (2014) 276–291.
[26] S. Lee, J. Kim, J. Lee, B.H. Cho, J. Power Sources 185 (2008) 1367–1373.
[27] J. Lee, J. Lee, O. Nam, J. Kim, B.-H. Cho, H.-S. Yun, S.-S. Choi, K. Kim, J.H. Kim, S. Jun, in: Proceedings of IEEE 12th International Power Electronics and Motion Control Conference (EPE-PEMC), 2006, pp. 1536–1540.
[28] J. Jang, J.-Y. Yoo, IEEE Trans. Energy Convers. 26 (2011) 290–298.
[29] J. Xu, C.C. Mi, B. Cao, J. Cao, J. Power Sources 233 (2013) 277–284.
[30] X. Li, J. Liu, X. Meng, Y. Tang, M.N. Banis, J. Yang, Y. Hu, R. Li, M. Cai, X. Sun, J. Power Sources 247 (2014) 57–69.
[31] J. Kim, B.H. Cho, Energy 57 (2013) 581–599.